

# Categorizing Cubes: Revisiting Pose Normalization

Mohsen Hejrati  
University of California, Irvine  
shejrati@ics.uci.edu

Deva Ramanan  
Carnegie Mellon University  
deva@cs.cmu.edu

## Abstract

*This paper introduces and analyzes the novel task of categorical classification of cuboidal objects - e.g., distinguishing washing machines versus filing cabinets. To do so, it makes use of recent methods for automatic alignment of cuboidal objects in images. Given such geometric alignments, the natural approach for recognition might extract pose-normalized appearance features from a canonically-aligned coordinate frame. Though such approaches are extraordinarily common, we demonstrate that they are **not optimal**, both theoretically and empirically. One reason is that such approaches require accurate shape alignment. However, even with ground-truth alignment, pose-normalized representations may still be sub-optimal. Instead, we introduce methods based on pose-synthesis, a somewhat simple approach of augmenting training data with geometrically perturbed training samples. We demonstrate, both theoretically and empirically, that synthesis is a surprisingly simple but effective strategy that allows for state-of-the-art categorization and automatic 3D alignment. To aid our empirical analysis, we introduce a novel dataset for cuboidal object categorization.*

## 1. Introduction

This paper examines geometric representations for 3D shape categorization, focusing on cuboidal object categories such as washing machines, cabinets, etc. We specifically focus on the task of *categorization* (“is this a washing machine or a cabinet?”), but demonstrate that our developed representation also produce competitive estimates of *3D shape* (“where are the corners of its faces?”) Cuboidal objects are interesting since they share the same basic shape, allowing one to explicitly explore the interplay of geometry and appearance.

**Alignment:** Aligning 3D models to images is a classic problem in computer vision, dating back to model-based techniques such as geometric hashing [19]. Combining such approaches with data-driven statistical models have proven quite effective [28, 23, 39, 17, 24, 29]. Most related

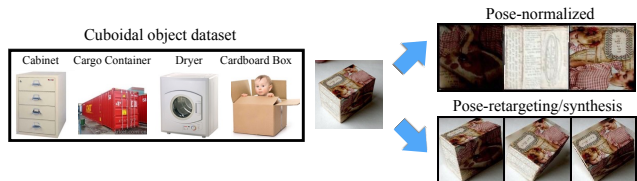


Figure 1. We examine categorization of cuboidal objects (**left**) into washing machines, cabinets, etc. Such objects share similar shape, so conventional wisdom might advocate the use of shape-invariant (or pose-normalized) representations for recognition (**top**). Such approaches are attractive because they (1) factor out shape (which seems uninformative when classifying objects with similar shape) and (2) can generalize to novel shapes not encountered in training data. We show that this strategy is not optimal. One reason is that current methods produce small errors in geometric alignment, which can result in large fluctuations in the pose-normalized appearance. However, even with ground-truth alignment, pose-normalization is still not optimal. We demonstrate that pose-synthesis (**bottom**), a simple approach of augmenting training data with geometrically perturbed training samples, is a surprisingly effective strategy that allows for state-of-the-art categorization and automatic 3D alignment.

to us are methods that focus on cuboidal objects, motivated by their generality and usefulness for describing many common objects [11, 35, 10, 14]. Interestingly, cuboidal alignment has also proven helpful for analyzing indoor scenes of cuboidal rooms [8, 6, 26, 9]. We build on such work by attempting the natural “next step”: how should one use one of the aforementioned geometric-alignment engines to recognize different *categories* of cuboidal objects?

**Pose-normalization:** Perhaps the most natural approach would use the estimated alignment to extract *pose-normalized* appearance features. For a cuboidal object, one might represent the appearance of each cuboidal face in a fronto-parallel view (Fig. 1). Many state-of-the-art systems for recognition (such as faces [31, 16], cars [17], animal species [2, 7], or general attributes [37]) similarly normalize landmarks/keypoints into a canonical coordinate frame during training and or testing. For example, the vast majority of face recognition systems work by detecting landmarks, warping the image such that landmarks are aligned into a

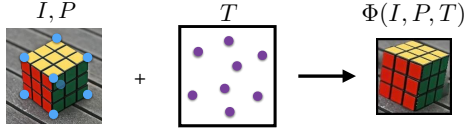


Figure 2. Proposed image-based rendering engine takes an image  $I$ , a set of 2D landmarks  $P$  and a set of target 2D landmark locations  $T$  as input, then it renders the cube in target view by warping each surface using a homography warp.

canonical frontal view (sometimes known as *frontalization*), and classifying the pose-normalized appearance [38, 13]. Importantly, normalization allows one to (1) factor out “nuisance” variables such as viewpoint and aspect/shape during recognition, and (2) generalize to viewpoints/poses not seen in training data.

**Pose-retargeting:** First and foremost, we demonstrate that pose-normalization is *not* the optimal strategy for dealing with appearance variation due to pose. One explanation maybe the inaccuracy of current systems for pose estimation - small misalignments in the predicted pose may cause large errors in the pose-normalized appearance. Surprisingly, we show that *even with ground-truth alignment on test images*, pose-normalization is still not optimal. In short, pose-normalization (a) removes geometric cues that maybe helpful for recognition (washing machines may have differing aspect ratio from microwaves) and (b) artificially re-weights foreshortened regions of the objects. To address these limitations, we describe a novel approach that *retargets* training examples by warping them “on-the-fly” to the shape and viewpoint of a particular detected instance, and performs recognition using this retargeted training set.

**Pose-synthesis:** While pose-retargeting is optimal given ground-truth alignment, its performance suffers when using an automated alignment that may contain some errors. To allow for imprecise alignment, we evaluate another approach that *pre-synthesizes* a large set of possible target poses. The synthesized set is used to train a practical system that jointly performs categorization *and 3D alignment*. Perhaps surprisingly, we demonstrate that such methods even outperform state-of-the-art systems for 3D alignment. Importantly, synthesis also allows our system to generalize to unseen viewpoints and shapes *without* requiring pose-normalization.

**3D data-augmentation:** Our proposed approaches are inspired by learning architectures that apply synthetic perturbations to training data. Such “data-augmentation” appears to be crucial components of state-of-the-art methods like deep learning [22, 18]. However, instead of applying simple perturbations like rotations, we make use of an image-based rendering engine to generating new 3D shapes and viewpoints (using piecewise-constant homographies

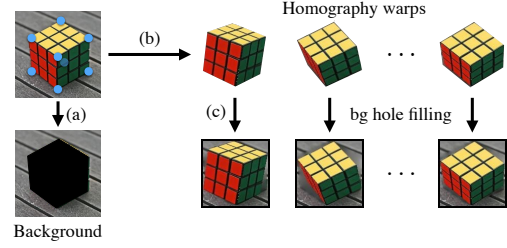


Figure 3. The image-based rendering engine works in three steps: (a) extracting background from the image. (b) rendering object in different poses using homography warps on object surfaces. (c) pasting the warped object on the background and filling the the holes using interpolation.

and affine transformations). With a rich enough synthesis engine, the resulting learning algorithm does not need to generalize to unseen test poses (because they can be directly synthesized). Indeed, we show that highly-invariant appearance features based on contemporary CNNs [27] may not outperform traditional gradient orientation histograms [5] when used with large synthetic training sets.

**Model-based synthesis:** Our retargeting and synthesis approaches can be seen as the “data-driven” counterpart to “model-based” approaches that warp a 3D categorical model to match an image [1, 34, 11, 12, 25]. But instead of performing a search over 3D model parameters at test time (which is often gradient-based and maybe prone to local minima [20]), we *compile* 3D models into an augmented training set of 2D images. In that respect, our approach is similar to those that train on synthetically-rendered images of 3D CAD models [21, 28]. But crucially, we make use of “image-based” synthesis [15], making it easier to generate realistic-looking synthetic images. Indeed, we see 3D data-augmentation as one simple avenue for injecting 3D knowledge into data-driven architectures such as CNNs.

**Our contributions:** We compare, both theoretically and empirically, different representations for the novel task of categorizing cuboidal objects. We begin with a baseline pose-“agnostic” approach (that trains a categorical classifier agnostic to the pose of training/test data). We compare such a method with pose-normalization, pose-synthesis, and pose-retargeting (which to our knowledge, is novel). We provide two salient conclusions: (1) The novel problem of categorical cuboid classification provides an interesting testbed for solving a practical task while investigating the role of shape and geometry. To spur future research in this area, we re-purpose an existing dataset [35] (designed for for cuboidal detection and alignment) for the task of cuboidal category recognition by making use of category labels and adding 3D landmark annotations. (2) Pose-retargeting, both at test and train-time (through synthesis), provides a simple approach for dealing with geometric variation that significantly outperforms the widely-used pose-

normalization technique.

This paper is organized as follows. Section 2 describes our image-based rendering engine. Section 3 discusses our four representations in detail and theoretical motivation for Pose-Retargeted and Pose-Synthesis. Section 4 concludes with our experimental results.

## 2. Image-based rendering

The core computational engine of all our studied approaches is an image-based renderer that takes an  $H \times W$  input image  $I$ , a set of  $N$  2D landmarks  $P$ , and produces a warped image with a retargeted set of  $N$  landmarks  $T$  (Fig. 2). We write this engine as a function that returns an image:

$$\Phi(I, P, T), \quad I \in \mathcal{R}^{H \times W \times 3}, \quad P, T \in \mathcal{R}^{2 \times N} \quad (1)$$

Importantly, landmarks and their associated faces are assumed to have a semantic ordering. For example, the first face is the front of the washing machine, while the second is the top, etc. The warped image  $\Phi$  is synthesized in three stages: foreground synthesis, hidden surface synthesis, and background synthesis. Figure 3 illustrates each step of our rendering process.

**Foreground:** By triangulating the points, one could generate a retargeted image by applying affine warps to each triangle. Instead, we assume that the points will always be corners of a cuboidal object, and so can be connected onto quadrilateral faces instead of triangles. Our rendering engine applies a homography (which can be estimated by the 4 corners of a quadrilateral) to each quadrilateral face.

**Hidden-surfaces:** If target pose is very different from the input pose, then previously occluded cube faces may now become visible. We assume that objects are symmetric in appearance, and use the texture map from the opposite face as a replacement.

**Background:** We only warp pixels inside the input object to the target pose, leaving background pixels intact. This will result in holes in the background of the target image. We use standard hole-filling algorithms [4].

Our image-based-synthesis engine is fairly straightforward, similar in complexity to a typical homework assignment in an undergraduate computer vision course! [30]. Nevertheless, it produces startlingly photo-realistic images of cuboidal objects (Fig. 1). We use it to explore a variety of representations for geometric-invariant recognition.

## 3. Approaches

In this section, we describe a simple mathematical formalism for unifying all the geometric representations that we will consider. Throughout this section, we visualize the function  $\Phi$  as a warped image, but to simplify notation,

we assume that  $\Phi$  directly extracts a  $N$ -dimensional feature vector extracted from the warped image. We will explore oriented gradient features and deep features. Though these features will be used in a variety of classification engines – including nearest neighbor (NN) matching and SVMs – we write out the mathematical formulation for a simpler NN classifier below. We assume that we have a training set of *real* images where the  $i^{th}$  image is associated with a category label  $y_i$  and ground-truth landmarks  $P_i$ . We also assume that we have a *real* query image at test-time  $I$ , with an associated set of test-time landmarks  $P$ :

$$\text{Training images: } \{(I_i, y_i, P_i)\} \quad \text{Test image: } (I, P) \quad (2)$$

Test-time landmarks are typically provided by an automatic system [11], though we crucially also consider ground-truth landmarks. Finally, we also consider representations that do not require 2D landmarks. To denote such methods, we use the notation of  $\Phi(I, P, P) = \Phi(I, \cdot, \cdot)$  to specify an identity warp (where in fact, the set of points  $P$  need not be specified).

The simplest approach would be to simply ignore pose as an explicit confounding factor, and match using features extracted from un-warped images, as shown in the first row of Fig. 4:

$$\begin{aligned} \text{Pose-Agnostic}(I) &= y_{i^*} \\ i^* &= \arg \min_i \|\Phi(I_i, P_i, P_i) - \Phi(I, P, P)\|^2 \\ &= \arg \min_i \|\Phi(I_i, \cdot, \cdot) - \Phi(I, \cdot, \cdot)\|^2 \end{aligned} \quad (3)$$

where we use the second line to emphasize the fact the identity warp computed by  $\Phi$  did not require the knowledge of any landmarks. The first line will be useful for comparison with other approaches that do make use of landmarks. Such agnostic approaches can still be successful if the training set of images spans enough variations in pose. However, such methods fundamentally cannot generalize to novel poses at test-time, unless a highly invariant feature descriptor is used (e.g., bag-of-word representations [36]), in which case discriminability may suffer.

Pose-normalization warps both the training and query images into a canonical configuration of  $N$  landmarks  $C$ :

$$\begin{aligned} \text{Pose-Normalized}(I) &= y_{i^*} \\ i^* &= \arg \min_i \|\Phi(I_i, P_i, C) - \Phi(I, P, C)\|^2 \end{aligned} \quad (4)$$

We visualize our canonical configuration of cuboid face landmarks in Fig. 7. Pose-Normalized explicitly factors out viewpoint and shape (which is helpful if they serve as nuisance variables for categorization), and trivially generalizes to novel viewpoints and shapes not seen in the training set, illustrated in the second row of Fig. 4. Our experiments will show that normalization performs well when







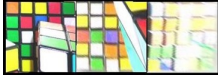











Method	Train: $I_i$	Rendered	Rendered	Query: $I$
Pose Agnostic		$\Phi(I_i, P_i, P_i)$ 		$\Phi(I, P, P)$ 
Pose Normalized		$\Phi(I_i, P_i, C)$ 		$\Phi(I, P, C)$ 
Pose Retargeted		$\Phi(I_i, P_i, P)$ 		$\Phi(I, P, P)$ 
Pose Synthesis		$\Phi(I_i, P_i, P_i^1)$  $\Phi(I_i, P_i, P_i^2)$  $\vdots$ $\Phi(I_i, P_i, P_i^K)$ 		$\Phi(I, P, P)$ 

Figure 4. We visualize various strategies for achieving geometric-invariance in recognition. Please refer to the text for a detailed description of each strategy.

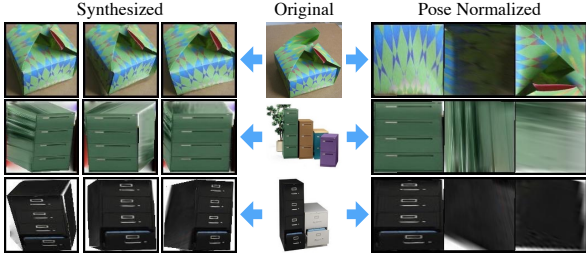


Figure 5. Given an image of an object, we show novel synthesized views generated by Pose-Synthesis (**left**) and the normalized view used by Pose-Normalized (**right**). Synthesized views look fairly realistic (because we can explicitly control and limit the degree of view synthesis), while the normalized views often have pixelation artifacts. The artifacts can arise from extrapolation of heavily-foreshortened cube faces (**middle row**) or small mistakes in the predicted 2D landmarks (**bottom row**).

given highly accurate alignments. Small errors in the estimated pose may cause large distortions in the normalized image (Fig. 8). However, even given ground-truth landmarks, pose-normalization may still artificially re-weight foreshortening portions of the object, sometimes resulting in image distortion due to pixelation artifacts (Fig. 7).

Instead of warping each training image to a canonical landmark configuration  $C$ , pose-retargeting warps each training image to the target landmarks  $P$  found on a query image  $I$ , as shown in Fig. 4:

$$\text{Pose-Retargeted}(I) = y_{i^*}$$

$$i^* = \arg \min_i \|\Phi(I_i, P_i, P) - \Phi(I, P, P)\|^2 \quad (5)$$

In some sense, pose-retargeting creates an “on-the-fly” custom-training set for this particular query image by warping the training set into the viewpoint and shape of the query. This tends to produce less distortions because warps are applied to training images (which tend to be cleaner and more accurately labeled landmarks) rather than a test-image. However, retargeting still requires accurate alignment landmarks at test-time, and more-over, may be slower since it requires generating a custom training set for each query.

Finally, we also consider an alternative that pre-warps all training images to set of possible target shapes and viewpoints. Pose-synthesis representation is based on augmenting the train set with new views of the training images (Fourth row in Fig. 4):

$$\text{Pose-Synthesis}(I) = y_{i^*}$$

$$i^* = \arg \min_i \min_{P_i^k \in G(P_i)} \|\Phi(I_i, P_i, P_i^k) - \Phi(I, P, P)\|^2$$

$$(i^*, P_i^{k^*}) = \arg \min_{i, P_i^k \in G(P_i)} \|\Phi(I_i, P_i, P_i^k) - \Phi(I, \cdot, \cdot)\|^2 \quad (6)$$

where  $G(P_i) = \{P_i^1, \dots, P_i^K\}$  generates a set of candidate target landmarks. We refer to this function as a *landmark-synthesis* engine, described further below. We rewrite the matching function as (6) to emphasize that (1) Pose-Synthesis does not require landmarks to be annotated



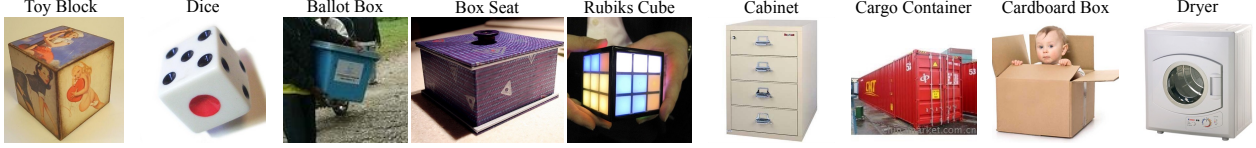


Figure 6. Our dataset of cuboidal object categories, re-purposed from the SUN Primitive database [35]. This dataset includes variation in shapes (aspect ratios), viewpoint, backgrounds and clutter.

on test images and (2) Pose-Synthesis can also be used for 3D landmark prediction ( $P_i^{k*}$ ).

**Landmark synthesis:** Landmark synthesis is used to generate a set of reasonable target landmarks for each training image  $I_i$ , to be used by Pose-Synthesis. We assume that each training image is labeled with 3D landmarks (in camera coordinates) and a focal length  $f$ . Specifically, 2D landmarks  $P$  are assumed to be perspective projection of the 3D points:

$$P_i = \text{Project}(S_i, f_i) \\ P_i \in \mathcal{R}^{2 \times N}, S_i \in \mathcal{R}^{3 \times N}, f_i \in \mathcal{R}$$

We use nonrigid structure-from-motion [11, 32] to infer 3D landmarks (and affine camera parameters) from 2D annotations. We use these estimates to then infer a perspective camera calibration to produce  $f_i$ . Given 3D shape and camera parameters, we generate rotations along the camera  $x$  and  $z$  axis:

$$G(P_i) = \{\text{Project}(R_k S_i, f_j)_{k=1}^K\} \\ R_k \in \mathcal{R}^{3 \times 3}, R_k^T R_k = I$$

In our experiments, we uniformly sample  $R_k = R_z R_x$  by ranging  $R_x$  and  $R_z$  over increments of  $(-15, 0, 15)$  degrees.

**Other synthesis strategies:** We explored other synthesis strategies for Pose-Synthesis. For example, one could generate aspect ratio variations in the set of shapes  $G$ . Moreover, one could extend the notion of data augmentation into the appearance domain as well as shape. For example, we could synthesize hidden cube surfaces or backgrounds by swapping out surfaces and backgrounds from other training examples. Our experiments focus on viewpoint synthesis, but our encouraging results suggest that other synthesis techniques are worth exploring.

**Theoretical analysis:** We now provide a simple theoretical motivation of Pose-Retargeted and Pose-Synthesis. Consider a generative model of an image as

$$Pr(\text{Image}, \text{Pose}) = Pr(\text{Pose})Pr(\text{Image}|\text{Pose}) \quad (7)$$

which is equal to

$$Pr(\text{Pose})\mathcal{N}(\text{Image}; \Phi(I, C, \text{Pose}), \sigma^2 Id) \\ \text{for } \mathcal{N}(x; \mu, \Sigma)$$

where  $I$  is image of the cuboidal faces in a canonical training view  $C$  and  $Id$  is the identity matrix. The above model generates a (pose,image) pair by warping a fronto-parallel view of a cube to a random pose and adding Gaussian noise to the warped image.

It is straightforward to show that Pose-Synthesis matches an image using the log-probability of that image under (7), (max) marginalizing over an uninformative pose prior:

$$I^*, \text{Pose}^* = \arg \max_{I \in \text{train}, \text{Pose}} Pr(\text{Image}, \text{Pose}) \quad (8)$$

The category label is defined by label of  $I^*$  available in training and estimated pose is  $\text{Pose}^*$ . Pose-Retargeted uses the log-probability of  $P(\text{Image}|\text{Pose})$ , conditioning on the known pose:

$$I^* = \arg \max_{I \in \text{train}} Pr(\text{Image}|\text{Pose}) \quad (9)$$

Intuitively, both Pose-Retargeted and Pose-Synthesis score an image reconstruction error that searches over candidate poses or conditioned on a known pose.

## 4. Experimental Results

**Dataset:** We re-purpose the SUN Primitive dataset [35], containing 1269 cuboid objects (annotated with 2D corners) in 785 images. SUN Primitive was proposed to study cuboid detection and 2D alignment. We use a subset of 543 cuboids that have category labels, spanning a set of 9 categories (Fig. 6). To apply our synthesis algorithms, we generate 3D landmark annotations for this dataset using the method described above. We use a 50-50 split for training and testing. While somewhat small by contemporary standards, this dataset provides a starting point for evaluating this novel problem, while allowing us to compare with previous published systems that were used to benchmark cuboid detection and alignment accuracy. We will release our 3D annotations to spur further research. Due to space restrictions, we provide additional diagnostic analysis (such as class-confusion matrices and localization results) in supplementary material.

**Features:** We evaluate oriented gradient descriptors (HOG) [5] and state-of-the-art convolutional neural net (CNN) features [18] when defining our final image descriptors  $\Phi$ . We resize images to 128x128 pixels before extracting features. For Pose-Normalized, we extract a feature de-



Figure 7. 3D landmarks predicted from Pose-Synthesis, following (6)

scriptor for each face of the normalized cuboid (concatenating them together to produce  $\Phi$ ). We use standard implementations of HOG and Oxford’s Deep19 CNN model [27], as implemented in the MatConvnet library [33]. We experiment with features extracted from different neural layers, finding the third convolutional layer to perform best.

**Classifiers:** We describe our representations using a nearest-neighbor (NN) formulation (Sec. 3), but the associated feature vectors  $\Phi$  can be used with any classification system. We explore SVMs as an alternate state-of-the-art classifier, considering both linear and Gaussian kernels where hyperparameters are selected through 5-fold cross-validation. We make use of the LIBSVM [3] library. When the category model need not generalize across different poses (which is true for Pose-Normalized and Pose-Retargeted), linear classifiers appear to suffice. Pose-Agnostic and Pose-Synthesis must reason across viewpoints, and so Gaussian kernels were vital for good performance.

**Landmark prediction:** We use a state-of-the-art cuboid landmark detection method [11] to estimate 2D landmarks at test-time (needed for Pose-Normalized and Pose-Retargeted). Importantly, this system has been shown to produce state-of-the-art alignment results on the SUN Primitive dataset, outperforming prior work such as [10, 35]. We show that some of our simple methods even outperform this body of work, in terms of landmark predictions. To simplify our analysis, we assume that a ground-truth bounding-box is provided at test-time for all experiments (including when running the system of [11]).

**Categorization:** Fig. 9 evaluates all approaches for object categorization accuracy, for both sets of features (CNN and HOG) and classifiers (SVM and NN). We plot confusion matrices and example mistaken images in the supplementary material. We discuss some conclusions below.

**Normalization:** Pose-Normalized performs the worst of all methods, no matter the feature or classifier. One immediate explanation could be that the predicted landmarks of [11] are not of sufficient accuracy. To test this hypothesis, we also evaluate accuracy given ground-truth landmarks. In

this setting, Pose-Normalized *does* perform the best out of all methods. Hence one immediate conclusion is that current alignment systems are not of sufficient accuracy to realize the benefits of a pose-normalized representation. In general, we see a significant 11% drop in accuracy in using predicted versus ground-truth landmarks.

**Retargeting:** However, in almost all cases, Pose-Retargeted outperformed Pose-Normalized, validating our initial hypothesis that normalization (1) is more susceptible to errors in landmark predictions and (2) artificially weights/distorts foreshortened regions of the object. One might think of Pose-Retargeted with ground-truth (GT) landmarks as an upper bound of Pose-Synthesis, because a perfect synthesis strategy should generate exactly those shapes that align with test images. Interestingly, Pose-Synthesis outperforms Pose-Retargeted-GT with CNN features. Because CNN features are invariant to large spatial deformations, we posit that the learned model can still benefit from a larger training set that includes shapes outside the testset.

**Agnostic vs Synthesis:** Overall, we find that Pose-Agnostic performs quite well, consistently outperforming Pose-Normalized and Pose-Retargeted when using predicted landmarks. We attribute this behavior again to the fact that highly accurate landmarks are needed for reliable alignment. However, Pose-Agnostic will struggle to generalize to a viewpoint or shape not seen in the training set. Pose-Synthesis is attractive because it offers generalization without sensitivity to geometric mis-alignment.

**Training data:** Because Pose-Normalized may perform relatively better with limited training data (making generalization to unseen views more important), Fig. 10 plots the accuracy of all methods for differing amounts of real training images. As expected, all methods do better with more data. Pose-Synthesis makes the most of additional data, producing a 15% improvement on average (probably because each additional training sample effectively adds 9 more view-perturbed examples). Agnostic, Retargeting and Normalized see average improvements of 12.7%, 9.8% and 6.5% respectively.

**Landmark localization:** To evaluate landmark localization, we use standard approach of counting the number of correctly localized landmarks. A landmark is correctly localized if it lies within  $t$  pixels of the ground-truth location, where  $t = 15\%$  of the square root of the area of the ground-truth box. We use NN-variants of our Pose-Agnostic and Pose-Synthesis models to generate landmark predictions, simply reporting back landmarks associated with the closest-matching training image (be it a real image or a synthesized one). Fig. 11 and Fig. 12 shows the result of our proposed approaches compared to the state-of-the-art. Both Pose-Agnostic (84.2%) and Pose-Synthesis (83.2%) significantly outperform the state-of-the-art method of [11]

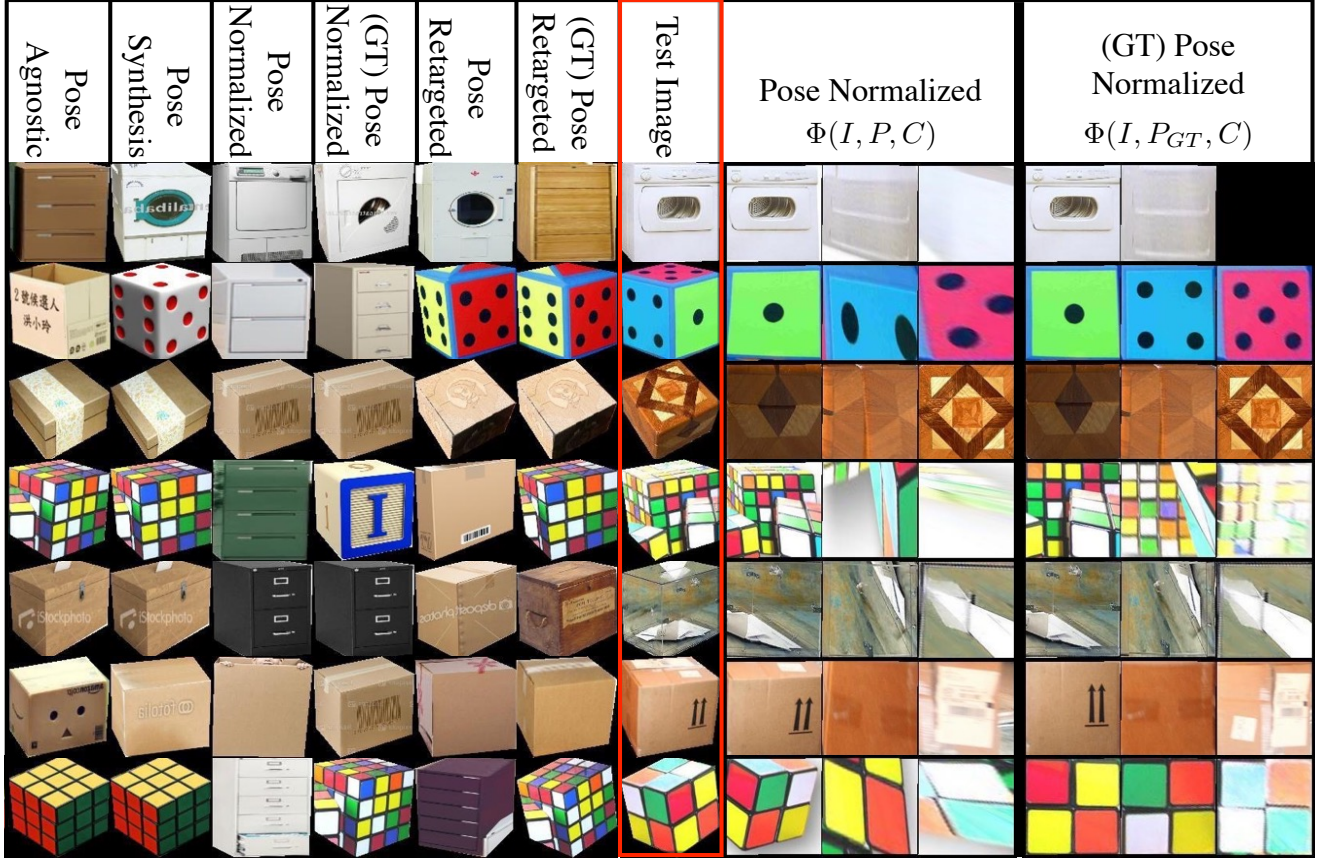


Figure 8. The **center red** column designates a test image, while the first six correspond to the NN-matches using our various representations. On the **right**, we visualize both the automatically-generated and ground-truth normalized image. Note how erroneous alignment create significant fluctuations in pose-normalized image, causing wrong NN-matches. Provided ground-truth alignment, pose-retargeting performs the best, while pose-synthesis performs best using automatic alignment. We include additional such visualizations in supplementary material.

Feature Classifier	HOG NN	HOG SVM	CNN NN	CNN SVM
Pose-Agnostic	43.3	58.9	42.6	56.3
Pose-Normalized	36.3	48.1	35.9	41.9
Pose-Retargeted	43	54.4	38.1	43.7
Pose-Synthesis	47.4	57.3	47	<b>59.6</b>
Pose-Normalized (GT)	46.7	<b>63</b>	44.4	54.1
Pose-Retargeted (GT)	54.8	62.2	45.9	56.7

Figure 9. Categorization accuracy of various approaches. Chance performance on this 9-class task is roughly 11%. The top-four methods are fully automatic, making use of predicted landmarks from Hejrati and Ramanan [11] when needed. The bottom-two make use of ground-truth (GT) landmarks.

(77.5%), which itself outperformed numerous other approaches on this dataset [10, 35]. With enough (real) training images, simply using real training data (Pose-Agnostic) performs quite well. But with a small number of real images (10) per category, Pose-Synthesis significantly outperforms

both Pose-Agnostic and prior art.

**Conclusion:** We provided theoretical and empirical analysis of different representations for the novel task of categorizing cuboidal objects, examining Pose-Agnostic, Pose-Normalized, Pose-Retargeted, and Pose-Synthesis-based models. We show that the problem of categorical cuboid classification is a useful testbed for investigating the interplay of shape and geometry while solving a practical task. Our theoretical and empirical analysis reveals the surprising result that Pose-Retargeting and Pose-Synthesis provides a simple approach for dealing with geometric variation that significantly outperforms the common-place technique of Pose-Normalization.

## References

- [1] V. Blanz and T. Vetter. A morphable model for the synthesis of 3d faces. In *Proceedings of the 26th annual conference on Computer graphics and interactive techniques*, pages 187–194. ACM Press/Addison-Wesley Publishing Co., 1999.



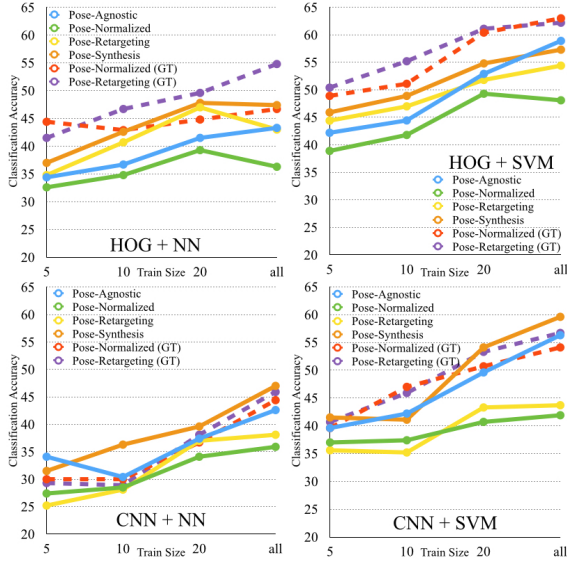


Figure 10. Accuracy of all methods for differing amounts of real training images.

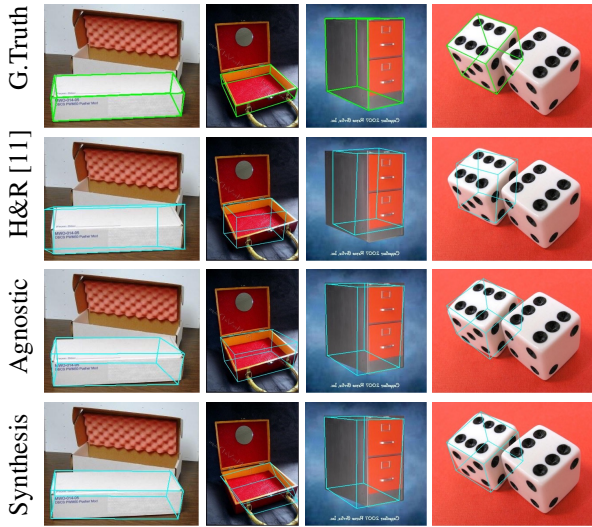


Figure 11. Samples of our landmark localization results. We compare the approach of Hejrati and Ramanan [11] with Pose-Agnostic and Pose-Synthesis (and the Ground-Truth). With a large amount of training data, Agnostic and Synthesis both outperform [11], though Synthesis does produce slightly better shape estimates because it can generalize to never-before-seen views and shapes (by synthesizing them). With less training data, this difference becomes much more pronounced - see Fig. 12.

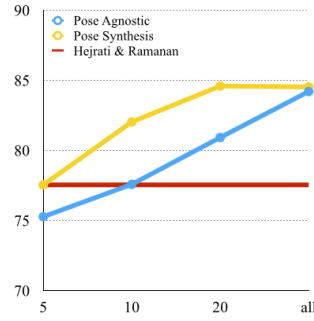


Figure 12. Landmark estimation accuracy of Pose-Synthesis and Pose-Agnostic (where we assume all training images have been annotated with landmarks), compared to the automatic approach of [11]. With enough (real) training images, simply using real training data (Pose-Agnostic) performs quite well. But with a small number of real images (10) per category, Pose-Synthesis significantly outperforms both Pose-Agnostic and prior art.

object removal by exemplar-based image inpainting. *Image Processing, IEEE Transactions on*, 13(9):1200–1212, 2004.

- [5] N. Dalal and B. Triggs. Histograms of oriented gradients for human detection. In *Computer Vision and Pattern Recognition, 2005. CVPR 2005. IEEE Computer Society Conference on*, volume 1, pages 886–893. IEEE, 2005.
- [6] L. Del Pero, J. Guan, E. Brau, J. Schlecht, and K. Barnard. Sampling bedrooms. In *Computer Vision and Pattern Recognition (CVPR), 2011 IEEE Conference on*, pages 2009–2016. IEEE, 2011.
- [7] R. Farrell, O. Oza, N. Zhang, V. I. Morariu, T. Darrell, and L. S. Davis. Birdlets: Subordinate categorization using volumetric primitives and pose-normalized appearance. In *Computer Vision (ICCV), 2011 IEEE International Conference on*, pages 161–168. IEEE, 2011.
- [8] A. Gupta, A. A. Efros, and M. Hebert. Blocks world revisited: Image understanding using qualitative geometry and mechanics. In *Computer Vision–ECCV 2010*, pages 482–496. Springer, 2010.
- [9] V. Hedau, D. Hoiem, and D. Forsyth. Thinking inside the box: Using appearance models and context based on room geometry. In *Computer Vision–ECCV 2010*, pages 224–237. Springer, 2010.
- [10] M. Hejrati and D. Ramanan. Analyzing 3d objects in cluttered images. In *Advances in Neural Information Processing Systems*, pages 593–601, 2012.
- [11] M. Hejrati and D. Ramanan. Analysis by synthesis: 3d object recognition by object reconstruction. In *Computer Vision and Pattern Recognition (CVPR), 2014 IEEE Conference on*, pages 2449–2456. IEEE, 2014.
- [12] S. Hinterstoisser, C. Cagniard, S. Ilic, P. Sturm, N. Navab, P. Fua, and V. Lepetit. Gradient response maps for real-time detection of textureless objects. *Pattern Analysis and Machine Intelligence, IEEE Transactions on*, 34(5):876–888, 2012.
- [13] A. K. Jain and S. Z. Li. *Handbook of face recognition*, volume 1. Springer, 2005.

- [2] S. Branson, G. Van Horn, S. Belongie, and P. Perona. Bird species categorization using pose normalized deep convolutional nets. *arXiv preprint arXiv:1406.2952*, 2014.
- [3] C.-C. Chang and C.-J. Lin. Libsvm: a library for support vector machines. *ACM Transactions on Intelligent Systems and Technology (TIST)*, 2(3):27, 2011.
- [4] A. Criminisi, P. Pérez, and K. Toyama. Region filling and



- [14] H. Jiang and J. Xiao. A linear approach to matching cuboids in rgb-d images. In *Computer Vision and Pattern Recognition (CVPR), 2013 IEEE Conference on*, pages 2171–2178. IEEE, 2013.
- [15] S. B. Kang, Y. Li, X. Tong, and H.-Y. Shum. Image-based rendering. *Foundations and Trends® in Computer Graphics and Vision*, 2(3):173–258, 2006.
- [16] Y. Kang, K.-T. Lee, J. Eun, S. E. Park, and S. Choi. Stacked denoising autoencoders for face pose normalization. In *Neural Information Processing*, pages 241–248. Springer, 2013.
- [17] J. Krause, M. Stark, J. Deng, and L. Fei-Fei. 3d object representations for fine-grained categorization. In *Computer Vision Workshops (ICCVW), 2013 IEEE International Conference on*, pages 554–561. IEEE, 2013.
- [18] Y. LeCun, L. Bottou, Y. Bengio, and P. Haffner. Gradient-based learning applied to document recognition. *Proceedings of the IEEE*, 86(11):2278–2324, 1998.
- [19] J. L. Mundy, A. Zisserman, et al. *Geometric invariance in computer vision*, volume 92. MIT press Cambridge, 1992.
- [20] M. H. Nguyen and F. D. La Torre. Local minima free parameterized appearance models. In *Computer Vision and Pattern Recognition, 2008. CVPR 2008. IEEE Conference on*, pages 1–8. IEEE, 2008.
- [21] B. Pepik, M. Stark, P. Gehler, and B. Schiele. Teaching 3d geometry to deformable part models. In *Computer Vision and Pattern Recognition (CVPR), 2012 IEEE Conference on*, pages 3362–3369. IEEE, 2012.
- [22] A. S. Razavian, H. Azizpour, J. Sullivan, and S. Carlsson. CNN features off-the-shelf: an astounding baseline for recognition. *arXiv preprint arXiv:1403.6382*, 2014.
- [23] S. Satkin, J. Lin, and M. Hebert. Data-driven scene understanding from 3d models. 2012.
- [24] S. Savarese and L. Fei-Fei. 3d generic object categorization, localization and pose estimation. In *ICCV*, 2007.
- [25] S. Savarese and L. Fei-Fei. View synthesis for recognizing unseen poses of object classes. In *Computer Vision–ECCV 2008*, pages 602–615. Springer, 2008.
- [26] A. G. Schwing, S. Fidler, M. Pollefeys, and R. Urtasun. Box in the box: Joint 3d layout and object reasoning from single images. In *Computer Vision (ICCV), 2013 IEEE International Conference on*, pages 353–360. IEEE, 2013.
- [27] K. Simonyan and A. Zisserman. Very deep convolutional networks for large-scale image recognition. *arXiv preprint arXiv:1409.1556*, 2014.
- [28] M. Stark, M. Goesele, and B. Schiele. Back to the future: Learning shape models from 3d cad data. In *BMVC*, volume 2, page 5, 2010.
- [29] M. Sun, H. Su, S. Savarese, and L. Fei-Fei. A multi-view probabilistic model for 3d object classes. In *CVPR*, pages 1247–1254. IEEE, 2009.
- [30] R. Szeliski. *Computer vision: algorithms and applications*. Springer Science & Business Media, 2010.
- [31] Y. Taigman, M. Yang, M. Ranzato, and L. Wolf. Deepface: Closing the gap to human-level performance in face verification. In *Computer Vision and Pattern Recognition (CVPR), 2014 IEEE Conference on*, pages 1701–1708. IEEE, 2014.
- [32] L. Torresani, A. Hertzmann, and C. Bregler. Nonrigid structure-from-motion: Estimating shape and motion with hierarchical priors. *Pattern Analysis and Machine Intelligence, IEEE Transactions on*, 30(5):878–892, 2008.
- [33] A. Vedaldi and K. Lenc. Matconvnet – convolutional neural networks for matlab. *CoRR*, abs/1412.4564, 2014.
- [34] J. Xiao, S. Baker, I. Matthews, and T. Kanade. Real-time combined 2d+ 3d active appearance models. In *CVPR (2)*, pages 535–542, 2004.
- [35] J. Xiao, B. Russell, and A. Torralba. Localizing 3d cuboids in single-view images. In *Advances in Neural Information Processing Systems*, pages 746–754, 2012.
- [36] J. Zhang, M. Marszałek, S. Lazebnik, and C. Schmid. Local features and kernels for classification of texture and object categories: A comprehensive study. *International journal of computer vision*, 73(2):213–238, 2007.
- [37] N. Zhang, M. Paluri, M. Ranzato, T. Darrell, and L. Bourdev. Panda: Pose aligned networks for deep attribute modeling. In *Computer Vision and Pattern Recognition (CVPR), 2014 IEEE Conference on*, pages 1637–1644. IEEE, 2014.
- [38] W. Zhao, R. Chellappa, P. J. Phillips, and A. Rosenfeld. Face recognition: A literature survey. *Acm Computing Surveys (CSUR)*, 35(4):399–458, 2003.
- [39] M. Z. Zia, M. Stark, B. Schiele, and K. Schindler. Detailed 3d representations for object modeling and recognition, 2013.